Walisongo Journal of Chemistry
Walisongo Journal of Chemistry Vol. 7 Issue 2 (2024), 245-253
ISSN: 2621-5985 (online); 2549-385X (print)
DOI: https://doi.org/10.21580/wjc.v7i2.24018

SYNTHESIS OF Fe_3O_4-ZnO-BENTONITE COMPOSITE AND THEIR ACTIVITIES IN PHOTODEGRADATION OF METHYLENE BLUE

Siti Nazilatul Amanah, Wirda Udaibah*, Kholidah

Department of Chemistry, Faculty of Science and Technology, Universitas Islam Negeri Walisongo Semarang, Indonesia

***Corresponding author:** wirdaudaibah@walisongo.ac.id

Abstract

The development of Fe_3O_4-ZnO-Bentonite photocatalyst material is crucial for the treatment of dye effluents, particularly in response to the rapid growth of the textile industry. Methylene blue, widely used as a textile dye, poses environmental challenges. The combination of bentonite, ZnO, and Fe_3O_4 was synthesized using the coprecipitation method to create a material capable of photodegrading methylene blue dye. Fe_3O_4-ZnO-Bentonite was synthesized using 2 g of bentonite, 8.19 g of $Zn(NO_3)_2 \cdot 6H_2O$, and $FeSO_4$:$FeCl_3$ weight ratios (in grams) of 4.170:4.055 (composite 1), 4.170:8.109 (composite 2), and 4.170:12.164 (composite 3). Characterization of the photocatalyst materials was conducted using X-ray diffraction (XRD), ultraviolet diffuse reflectance spectroscopy (UV-DRS), and scanning electron microscopy-energy dispersive X-ray (SEM-EDX) mapping. The Fe_3O_4-ZnO-Bentonite composite exhibited a crystalline structure, with band gap values of 2.94 eV (composite 1), 2.07 eV (composite 2), and 2.20 eV (composite 3). The morphology of the material was characterized by small and irregularly shaped chunks. Elemental analysis detected Fe, Zn, and Si peaks, confirming the even distribution of Fe_3O_4 and ZnO within the bentonite matrix. The synthesized Fe_3O_4-ZnO-Bentonite composite demonstrated enhanced photodegradation activity for methylene blue compared to the starting materials. Composite 3 exhibited the highest photocatalytic activity, achieving a degradation efficiency of 96.02% at a methylene blue concentration of 20 ppm (pH 9) within 60 minutes.

Keywords: *Fe_3O_4-ZnO-Bentonite, photocatalyst, methylene blue*

Introduction

The rapid development of industry has significantly impacted environmental pollution, particularly due to the use of textile dyes. Among these, methylene blue ($C_{16}H_{18}N_3SCI$) is known to be particularly harmful to aquatic environments. Its widespread use in large quantities leads to environmental contamination because of its high toxicity (Islammiyatia et al., 2022). Prolonged exposure to methylene blue has been linked to health issues such as allergies, nausea, skin and digestive tract irritation, cyanosis from inhalation, eye burns, limb paralysis, and tissue necrosis (Choi & Yu, 2019; Ristianingsih et al., 2020). The concentration of dyes in textile industry wastewater typically ranges from 20–30 mg/L (Ramadhannur et al., 2021). According to the Regulation of the Ministry of Environment and Forestry of the Republic of Indonesia Number 6 of 2021, the permissible quality standard for methylene blue in wastewater is 5 mg/L.

Consequently, treating dye effluents before discharge into the environment is essential.

Several methods have been employed for methylene blue effluent treatment, including adsorption, filtration, biodegradation, chlorination, and ozonation. A widely used alternative is photocatalysis, which has the advantage of not producing secondary pollutants, as it converts organic dye pollutants into CO_2, H_2O, and inorganic minerals (Ramadhannur et al., 2021; Szostak & Banach, 2019).

Photocatalysts often utilize semiconductor materials such as TiO_2, ZnO, SnO_2, Ag_2O, CdS, Fe_2O_3, and NiO (Balarak, 2019). Among these, ZnO is widely preferred due to its non-toxic nature, availability, affordability, high reduction potential, and superior electron mobility (Rahimi et al., 2022; Ramadhika et al., 2021). However, Tang et al. (2022) highlighted a drawback of pure ZnO: its low photocatalytic activity caused by the high recombination rate of photon-induced electron-hole pairs. To enhance the efficiency of the photocatalytic process, the recombination of electrons and holes must be minimized, which can be achieved through metal or metal oxide doping.

Iron oxide (Fe_3O_4) is one such material that can be combined with ZnO (Huang et al., 2020). Fe_3O_4 is widely utilized as a photocatalyst due to its non-toxic properties, stability, and effectiveness in extending photoresponse ranges (Huang et al., 2020). In addition, Xia et al. (2011) reported that the ZnO-Fe_3O_4 combination exhibits excellent photocatalytic activity by capturing excited electrons from ZnO, thereby reducing electron-hole recombination rates.

The application of Fe_3O_4-ZnO composites is often hindered by material agglomeration, which decreases photocatalytic efficiency. This issue can be mitigated by dispersing the composite onto materials with mechanical stability, such as zeolite, bentonite, chitosan, or kaolin (Riskiani et al., 2018). Bentonite, in particular, has versatile applications as an adsorbent, catalyst, adhesive, and catalyst support (Chen et al., 2015; Jiang et al., 2018; Rabiudin et al., 2022). As a catalyst support, bentonite enhances the performance of Fe_3O_4 and ZnO photocatalysts in photodegradation processes and serves as a carrier solid that facilitates and accelerates reactions between photocatalyst metal oxides and organic compounds (Suprihatin et al., 2021).

Based on the above explanation, this study aimed to improve the photodegradation efficiency of methylene blue using an Fe_3O_4-ZnO-Bentonite photocatalyst material synthesized via the coprecipitation method. Research on this composite material remains limited, especially concerning variations in $FeCl_3$ composition for Fe_3O_4, methylene blue concentrations, and photocatalyst contact times. Lowering the photocatalyst's bandgap energy and reducing its crystal size were expected to enhance its photocatalytic activity. Additionally, the mechanisms involved in pollutant removal were explored to provide insights into wastewater treatment using this photocatalyst.

Methodology

Materials

The materials used in this research were $Zn(NO_3)_2{\cdot}6H_2O$ powder (Merck), $FeSO_4{\cdot}7H_2O$ powder (Merck KGaA), $FeCl_3{\cdot}6H_2O$ powder (Merck), $AgNO_3$ 0.1 M solution, Indrasari bentonite powder, NH_4OH 10% solution, NH_4OH 0.5 M solution (Merck), distilled water (aquadest), ethanol 96% p.a, HCl 6 M solution (Merck), and methylene blue 100 ppm solution (Merck). The tools included a 100-mesh sieve, magnetic stirrer, oven, furnace, universal pH indicator, and analytical balance. The instruments used were XRD, UV-DRS, UV-Vis, and SEM-EDX Mapping.

Bentonite Preparation and Activation

100 g of bentonite was placed in an oven at 120°C for 3 hours, cooled, and then ground with a mortar and pestle before sieving through a 100-mesh sieve until smooth. 20 g of pulverized bentonite was refluxed with 200 mL of 6 M HCl solution at 105–108°C for 6 hours. The mixture was then filtered and washed with distilled

water until it was free of Cl^- ions (confirmed by testing with $AgNO_3$). The washed residue was dried in an oven at 120°C for 2 hours, followed by calcination at 500°C for 5 hours. The calcined bentonite was crushed to a fine powder using a mortar and pestle, sieved through a 100-mesh sieve, and characterized using XRD, UV-DRS spectrophotometer (ASTM, 2005), and FTIR (Artanti, 2022).

ZnO Preparation

ZnO synthesis was conducted using the precipitation method described by Artanti (2022). Specifically, 5 g of $Zn(NO_3)_2 \cdot 6H_2O$ was dissolved in 50 mL of distilled water and stirred with a magnetic stirrer at 300 rpm and 80°C for 1 hour. Subsequently, 5 mL of 0.5 M NH_4OH solution was added, and the mixture was stirred under the same conditions for an additional hour. A 0.5 M NH_4OH solution was then added dropwise until the pH reached 9, resulting in the formation of a precipitate. The precipitate was filtered using filter paper and washed with distilled water until the pH was neutral (pH 7). The washed precipitate was dried in an oven at 90°C for 4 hours and calcined at 450°C for 4 hours. Characterization was performed using XRD and a UV-DRS spectrophotometer.

Fe_3O_4 Preparation

The preparation of Fe_3O_4 was based on the method by Habib et al. (2019). 4.170 g of $FeSO_4 \cdot 7H_2O$ and 8.109 g of $FeCl_3 \cdot 6H_2O$ were dissolved in 25 mL of distilled water. Then, 60 mL of 10% NH_4OH solution was added while stirring with a magnetic stirrer at 90°C for 90 minutes. The resulting precipitate was washed with distilled water until the pH was neutral and then precipitated using a permanent magnet to expedite the decantation process. The precipitate was filtered using filter paper and dried in an oven at 80°C for 3 hours. Characterization was subsequently conducted using XRD and a UV-DRS spectrophotometer.

reparation of Fe_3O_4-ZnO-Bentonite Composite

The preparation of the Fe_3O_4-ZnO-Bentonite composite involved adding 2 g of bentonite into a 100 mL glass beaker, followed by stirring with a magnetic stirrer at room temperature for 10 minutes at a speed of 100 rpm. Subsequently, $FeSO_4 \cdot 7H_2O$ and $FeCl_3 \cdot 6H_2O$ were added with molar ratio variations of 1:1, 1:2, and 1:3. The specific weights used are shown in Table 1. A 5 mL aliquot of 0.5 M NH_4OH solution was then added and stirred with a magnetic stirrer for another 10 minutes at room temperature. Next, $Zn(NO_3)_2 \cdot 6H_2O$ with a constant weight of 8.91 g was introduced, and the mixture was stirred at 300 rpm at 85°C for 4 hours. During this process, 0.5 M NH_4OH solution was gradually added until the pH reached 9. The resulting precipitate was filtered and washed with ethanol to remove impurities until neutral pH was achieved, then calcined at 350°C for 3 hours. The composites prepared with different $FeSO_4$:$FeCl_3$ molar ratios were designated as follows: (1) Composite 1: $FeSO_4$:$FeCl_3$ molar ratio of 1:1, with constant bentonite and ZnO masses; (2) Composite 2: $FeSO_4$:$FeCl_3$ molar ratio of 1:2, with constant bentonite and ZnO masses; and (3) Composite 3: $FeSO_4$:$FeCl_3$ molar ratio of 1:3, with constant bentonite and ZnO masses. Further characterization of the composites was performed using XRD, SEM with EDX Mapping, and UV-DRS spectrophotometry.

Characterization

The crystal structures of ZnO, Fe_3O_4, composite 1, composite 2, and composite 3 were analyzed using a Bruker D2 Phaser X-ray diffraction (XRD) instrument with Cu Kα radiation (λ = 0.154056 Å). Measurements were conducted at 2θ angles ranging from 10° to 80°, and the crystallite size was calculated using the Scherrer equation. The energy band gaps of ZnO, Fe_3O_4, composite 1, composite 2, and composite 3 were analyzed at UV-Vis wavelengths of 200–800 nm using a Cary UV-2415 UV-DRS (Diffuse Reflectance Spectroscopy) spectrophotometer. Morphological characterization of the composites was performed using a Phenom World Scanning Electron Microscope (SEM) to observe their surface structures.

 | ISSN 2621-5985 (online) | ISSN 2549-385X (print)
Volume 7, Nomor 2, 2024

Elemental composition analysis was carried out using Energy-Dispersive X-ray (EDX) at a voltage of 15 kV and magnifications of 5,000x and 10,000x. Mapping was conducted to visualize the distribution of ZnO and Fe_3O_4 on the bentonite surface. UV-Vis spectrophotometric analysis at wavelengths of 400–700 nm was used to determine the maximum absorption of the samples. Absorbance values were compared before and after photodegradation for bentonite, ZnO, Fe_3O_4, composite 1, composite 2, and composite 3.

Results and Discussion

XRD Analysis

XRD patterns of activated bentonite demonstrated peaks at 2θ: 19.09°, 22.31°, 26.68°, 54.89°, and 62.86°. These peaks aligned with the JCPDS database No. 29-1499, indicating they were typical for montmorillonite-type bentonite (Putri, 2020). ZnO peaks were observed at the following 2θ angles: 31.79°, 34.46°, 36.27°, 47.56°, 56.63°, 62.87°, 66.37°, 67.96°, 69.09°, and 72.78°, as referenced in the JCPDS database No. 00-900-4178. The diffraction pattern of Fe_3O_4 photocatalysts is shown in Figure 1, with peaks at 2θ angles of 29.87°, 35.96°, 53.66°, 56.11°, and 61.50°, corresponding to the standard Fe_3O_4 XRD pattern (JCPDS No. 00-900-5837), which included peaks at 29.91°, 35.36°, 43.02°, 53.33°, 56.98°, and 62.48°. According to research conducted by Oktavia and Rohmawati (2022), the highest peak of Fe_3O_4 was located at an angle of 35.58°. The XRD analysis confirmed that the highest and widest peaks were at 2θ angles of 29.87°, 35.96°, and 61.50°, indicating the presence of Fe_3O_4 with an amorphous structure.

Figure 1 depicts that the composite peaks were similar to the diffraction pattern of Fe_3O_4. Composite 1 exhibited diffraction peaks at 2θ: 30.08°, 35.31°, 56.90°, and 62.47°. Composite 2 had peaks at 2θ: 29.87°, 35.31°, 56.76°, and 62.26°, while Composite 3 displayed peaks at 2θ: 29.88°, 35.24°, 56.76°, and 62.33°. The starting material bentonite showed peaks at 2θ: 19.09°, 22.31°, 26.68°, 54.89°, and 62.86°; Fe_3O_4 at 2θ: 29.87°, 35.96°, 53.66°, 56.11°, and 61.50°; and ZnO at 2θ: 31.79°, 34.46°, 36.27°, 47.56°, 56.63°, 62.87°, 66.37°, 67.96°, 69.09°, and 72.78°.

The highest peaks of bentonite, Fe_3O_4, and ZnO were observed at 2θ: 26.68°; 35.96°; and 36.27°, respectively. From the composite data, the peaks of ZnO and bentonite were only slightly visible, as their diffraction peaks overlapped with Fe_3O_4. The highest peaks of Composites 1, 2, and 3 were at 2θ: 35.31°, 35.31°, and 35.24°, respectively, which were close to the highest peak of Fe_3O_4 at 2θ: 35.96°. This finding indicated that Fe_3O_4 was the dominant component in the composites, with bentonite contributing less than ZnO and Fe_3O_4. Furthermore, the peaks of bentonite and ZnO were similar to those of Fe_3O_4.

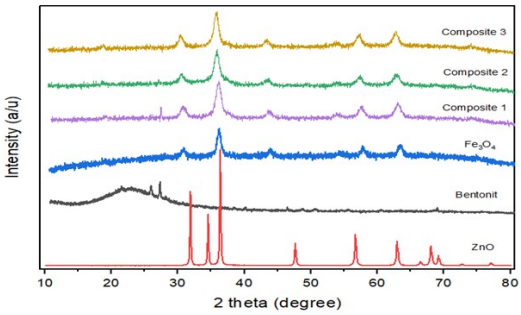

Figure 1. Diffractogram of Bentonite, ZnO, Fe_3O_4, and Fe_3O_4-ZnO-Bentonite composites

Based on Table 2, the average crystal sizes of the materials followed the order Fe_3O_4 > ZnO > bentonite > Composite 1 > Composite 2 > Composite 3. Increasing the Fe_3O_4 loading resulted in a decrease in crystal size. This finding aligned with research by Rahimi et al. (2022), who reported that higher Fe_3O_4 content could reduce the crystal size due to the increased loading of bentonite on ZnO. This reduction in crystal size increased the active sites of ZnO bonded to carbon. Smaller crystal sizes

were expected to enhance methylene blue photodegradation activity, as reduced crystal sizes might improve the photocatalytic interaction between the material and pollutants.

The energy gap was determined by constructing a curve relating (F(R)*hv)1/2 and energy (hv) as shown in Figure 2b. The synthesis results and calculations revealed the bandgap energy values followed the order as follows: ZnO > Composite 1 > Composite 3 > Composite 2 > Fe_3O_4. The bandgap energy for bentonite was not detected, as it was not a semiconductor material. The bandgap energy of Composites 1 and 2 decreased with the addition of $FeCl_3$ mol, while Composite 3 showed a slight increase compared to Composite 2. This was because the $FeCl_3$ mol addition in Composite 3 was optimal, expanding the photoresponse to visible light, narrowing the bandgap energy, and shifting the optical absorption range. However, if $FeCl_3$ mol was added beyond the optimum level, the excited Fe^{3+} interacted with the valence band, causing an increase in bandgap energy (Aprilita et al., 2022).

Table 1. Variation of Fe_3O_4-ZnO-Bentonite composites

Variation	$Zn(NO_3)_2{\cdot}6H_2O$ (g)	Bentonite (g)	$FeSO_4{\cdot}7H_2O$ (g)	$FeCl_3{\cdot}6H_2O$ (g)
Composite 1	8.91	2	4.170	4.055
Composite 2	8.91	2	4.170	8.109
Composite 3	8.91	2	4.170	12.164

Table 2. Average crystal size of Bentonite, Fe_3O_4, ZnO, and Fe_3O_4-ZnO-Bentonite composites

Photocatalyst	Crystal Size (nm)
ZnO	35.46
Fe_3O_4	36.34
Bentonite	27.14
Composite 1	7.93
Composite 2	6.74
Composite 3	6.73

UV DRS Analysis

Figure 2a shows that the wavelength followed the trend as follows: Bentonite < ZnO < Composite 1 < Composite 3 < Composite 2 < Fe_3O_4. This result indicated that doping Fe_3O_4 broadened the composite's photoresponse range to photons. The wider photoresponse range enhanced photocatalytic activity because more photon energy was absorbed by the material, leading to the formation of more electron-hole pairs. These electron-hole pairs played a crucial role in degrading methylene blue pollutants.

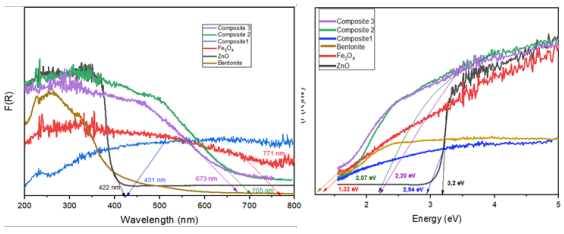

Figure 2. (a) Correlation between Wavelength and Kubelka-Munk Factor for ZnO, Fe_3O_4, and Fe_3O_4-ZnO-Bentonite Composite and (b) Bandgap Energy of Bentonite, ZnO, Fe_3O_4, and Fe_3O_4-ZnO-Bentonite Composite.

SEM-EDX Analysis

The morphological structure of the Fe_3O_4-ZnO-Bentonite composite was observed using SEM. Figure 3 shows the results, which consisted of smaller and irregular chunks. This finding was consistent with the research by Suprihatin et al, (2021), who successfully synthesized composites with similar morphological characteristics. EDX (Energy Dispersive X-ray) characterization data confirmed that the composite contained elements such as iron (Fe), zinc (Zn), oxygen (O), and silicon (Si). This result demonstrated the presence of Fe_3O_4, ZnO, and bentonite in the Fe_3O_4-ZnO-Bentonite composite, indicating that ZnO and Fe_3O_4 were evenly distributed on the bentonite surface. Detailed EDX data is provided in Figure 4. Additionally, the

Jurnal © 2024 WJC | ISSN 2621-5985 (online) | ISSN 2549-385X (print)
Volume 7, Nomor 2, 2024

mapping results in Figure 5 show the distribution of Zn, Si, Fe, C, and O in the composite, further confirming the uniform distribution of ZnO and Fe_3O_4 on the bentonite surface.

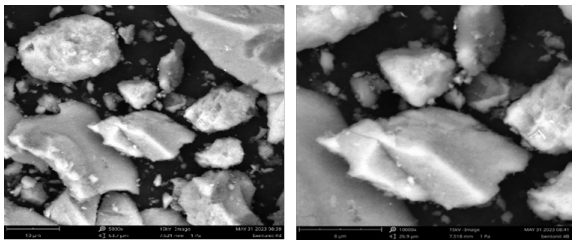

Figure 3. SEM Results of Fe_3O_4-ZnO-Bentonite at (a) 5000x magnification and (b) 10,000x magnification.

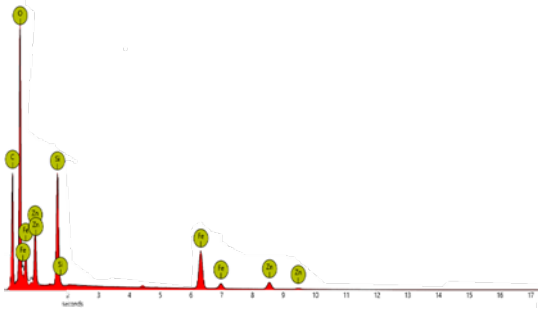

Figure 4. EDX results of Fe_3O_4-ZnO-Bentonite composite 3

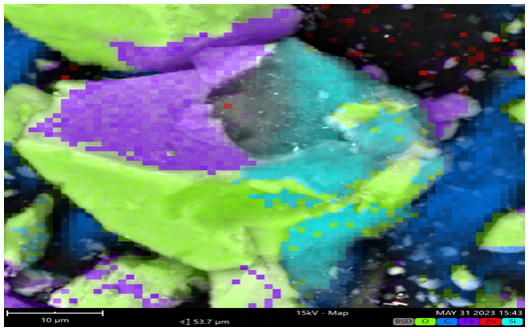

Figure 5. Mapping results for Fe_3O_4-ZnO-Bentonite composites

Photocatalytic Activity of Bentonite, ZnO, Fe_3O_4, and Fe_3O_4-ZnO-Bentonite in Methylene Blue Degradation

The morphological structure of the Fe_3O_4-ZnO-Bentonite composite was observed using SEM. Figure 3 displays the results, revealing smaller and irregular chunks. The photodegradation activity of methylene blue, as illustrated in Figure 6, followed the order as follows: Composite 3 > Composite 1 > Composite 2 > ZnO > Bentonite > Fe_3O_4. This finding indicated that the composite synthesis successfully enhanced the photocatalytic activity of the ZnO, bentonite, and Fe_3O_4 starting materials.

This finding was consistent with data obtained from XRD characterization, exhibiting the crystal size ranking as Fe_3O_4 > ZnO > Composite 1 > Composite 2 > Composite 3. Among the synthesized composites, composite 3 had the smallest crystal size despite having the highest molar ratio of $FeSO_4$ to $FeCl_3$ (1:3). This condition significantly affected the photodegradation of methylene blue. The photocatalytic activity of Fe_3O_4-ZnO-Bentonite was also affected by the band gap energy. Based on UV-DRS data and subsequent calculations, the band gap energy values were ranked as follows: ZnO > Composite 1 > Composite 3 > Composite 2 > Fe_3O_4. However, the energy gap of bentonite was not detected. For the synthesized composites, the gap energy followed the order as follows: Composite 1 > Composite 3 > Composite 2. A lower energy gap in the photocatalyst resulted in higher photocatalytic activity, facilitating the formation of electron-hole pairs from the conduction band to the valence band (Dehghan et al., 2018). Additionally, Fe_3O_4 had a smaller band gap energy than ZnO, which allowed Fe_3O_4 doping on ZnO to expand the photoresponse by increasing the absorption range. A higher $FeSO_4$:$FeCl_3$ molar ratio led to better activity. The percent degradation observed in composites 1 and 3 increased with the rise in $FeCl_3$ content within the composite.

This improvement was attributed to Fe_3O_4's ability to reduce electron recombination between the conduction band and the valence band. Reduced recombination could optimize OH formation, leading to more efficient degradation (Tao et al., 2019). Composite 2 had the smallest energy gap. A lower photocatalyst energy gap typically corresponds to higher photocatalytic activity. However, in this study, the

photocatalytic activity of Composite 2 indicated a reduced percentage of degradation compared to Composite 3. This reduction occurred because the small band gap energy caused the formation of a new band (mid-gap) that was too close to the conduction band. As a result, electrons were rapidly excited, leading to the rapid formation of O_2^-. The quick generation of O_2^- resulted in its reaction with continuously excited electrons and OH^- to form H_2O, which was ineffective in degrading methylene blue. Thus, it could be concluded that when the band gap energy of a photocatalyst was too small, the formation of O_2^- and OH^- became suboptimal, causing a decrease in the photocatalytic activity of Composite 2.

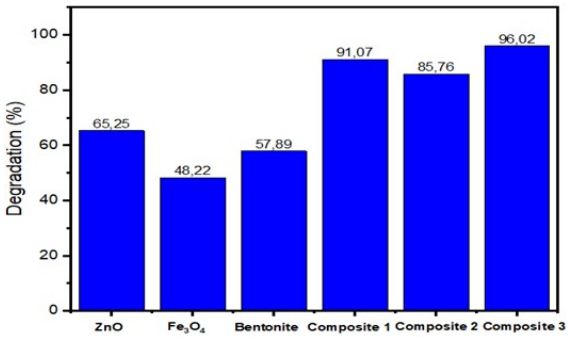

Figure 6. Effect of ZnO, Fe_3O_4, Bentonite, Composite 1, Composite 2, and Composite 3 on the photodegradation of methylene blue

Figure 7 shows the photocatalytic activity facilitated by UV light to form hydroxyl radicals (OH•) from water molecules and hydroxide ions. Hydroxyl radicals (OH•) acted as strong oxidizers that could degrade methylene blue dye. Electrons, separated into electrons and holes, reacted with organic substances or pollutants in water, resulting in their degradation into CO_2 and H_2O. Research conducted by Ramadhannur et al. (2021) demonstrated that the greater the production of hydroxyl radicals (OH•), the higher the degradation efficiency of methylene blue dye. The photocatalytic process occurring on the composite surface could be expressed as follows (Długosz et al., 2021):

$$\text{Bentonite-ZnO}\,(e^- + h^+) - Fe_3O_4\,(e^- + h^+) + h\nu \rightarrow \text{Bentonite-ZnO-}Fe_3O_4 + e^-(CB) + h^+(VB)$$

$$2\,h^+\,(VB) + 2\,H_2O \rightarrow 2H^+ + 2{\bullet}HO_2 \quad (1)$$

$$2\,e^-(CB) + 2\,O_2 \rightarrow 2{\bullet}O_2^- \quad (2)$$

$$2\,H^+ + 2{\bullet}O_2^- \rightarrow 2{\bullet}HO_2O_2 + e^- \rightarrow OH^{2-} \quad (3)$$

$$O^{2-} + H^+ \rightarrow {\bullet}HO_2 \quad (4)$$

$${\bullet}HO_2 \rightarrow H_2O_2 + O_2 \quad (5)$$

$$H_2O_2 + OH^{2-} \rightarrow OH{\bullet} + O_2 + OH^- \quad (6)$$

$$\text{Methylene blue} + OH \rightarrow CO_2 + H_2O \quad (7)$$

Figure 7. Diagram of electron and hole transfer in the system in the presence of dyes in solution

Conclusion

ZnO and Fe_3O_4-ZnO-Bentonite photocatalyst materials were crystalline solids that exhibited a peak shift, initially showing high peaks (indicative of crystallinity). Fe_3O_4 and bentonite, however, were classified as irregular amorphous solids. UV-DRS analysis indicated gap energy values of 3.20 eV, 2.94 eV, 2.07 eV, 2.20 eV, and 1.32 eV, while the gap energy of bentonite was not detected. SEM analysis revealed a morphology characterized by smaller and irregularly shaped chunks, while EDX mapping confirmed the presence of Fe, Zn, and Si elements evenly distributed on the bentonite surface. The photocatalytic activity of Fe_3O_4-ZnO-Bentonite was affected by crystal size and energy gap; smaller crystal sizes and lower energy gaps corresponded to higher photocatalytic activity. Among the composites, Photocatalyst 3 demonstrated the highest

photocatalytic activity, achieving a degradation efficiency of 96.02% in a 20 ppm methylene blue solution (pH 9) within 60 minutes.

References

Aprilita, N. H., Amalia, D., & Wahyuni, E. T. (2022). Removal of the Hazardous Congo Red Dye through Degradation under Visible Light Photocatalyzed by C,N Co-Doped TiO_2 Prepared from Chicken Egg White. *The Scientific World Journal*, *2022*, 14–17. https://doi.org/10.1155/2022/2613841

Artanti, D. (2022). *Sintesis dan Karakterisasi Komposit CuO-ZnO-Bentonit sebagai Kandidat Material Fotokatalis*.

Balarak, D. . F. K. (2019). Photocatalytic Degradation of Amoxicillin Using UV/Synthesized NiO from Pharmaceutical Wastewater. *J. Chem.* , *19*(1), 211–218.

Chen, W., Xiao, H., Xu, H., Ding, T., & Gu, Y. (2015). Photodegradation of Methylene Blue by TiO_2-Fe_3O_4-Bentonite Magnetic Nanocomposite. *Materials Chemistry and Physics*, *225*, 464–474. https://doi.org/10.1016/j.matchemphys.2018.11.029

Choi, H. J., & Yu, S. W. (2019). Biosorption of Methylene Blue from Aqueous Solution by Agricultural Bioadsorbent Corncob. *Environmental Engineering Research*, *24*(1), 99–106.

Dehghan, S., Kakavandi, B., & Kalantary, R. R. (2018). Heterogeneous Sonocatalytic Degradation of Amoxicillin using ZnO@Fe_3O_4 Magnetic Nanocomposite: Influential Factors, Reusability and Mechanisms. *Journal of Molecular Liquids*, *264*, 98–109. https://doi.org/10.1016/j.molliq.2018.05.020

Długosz, O., Wąsowicz, N., Szostak, K., & Banach, M. (2021). Photocatalytic Properties of Coating Materials Enriched with Bentonite/ZnO/CuO Nanocomposite. *Materials Chemistry and Physics*, *260*, 1–11. https://doi.org/10.1016/j.matchemphys.2020.124150

Habib, A., Ngatijo, & Gusti, D. R. (2019). Sintesis dan karakterisasi magnetit terlapis dimerkaptosilika. *Chempublish Journal*, *4*(2), 81–88. https://doi.org/10.22437/chp.v4i2.8034

Huang, C. Y., Tai, K. L., Huang, C. W., Tseng, Y. T., Lo, H. Y., & Wu, W. W. (2020). Dynamic observation on the functional metal oxide conversion behaviors in Fe_3O_4/ZnO heterostructures. *Scripta Materialia*, *177*, 192–197. https://doi.org/10.1016/j.scriptamat.2019.10.035

Islammiyatia, A., Azwar, A., & Asri, A. (2022). *Studi Pengaruh Penyinaran Lampu Ultraviolet pada Kinerja*. *10*(3), 430–435.

Jiang, L., Ye, Q., Chen, J., Chen, Z., & Gu, Y. (2018). Preparation of magnetically recoverable Bentonite–Fe_3O_4–MnO_2 composite particles for Cd(II) removal from aqueous solutions. *Journal of Colloid and Interface Science*, *513*, 748–759. https://doi.org/10.1016/j.jcis.2017.11.063

Kehutanan, M. L. H. dan. (2021). Peraturan Menteri Lingkungan Hidup Dan Kehutanan Republik Indonesia Nomor 6 Tahun 2021. *Menteri Lingkungan Hidup Dan Kehutanan Republik Indonesia*, *April*, 5–24.

Oktavia, A. D., & Rohmawati, L. (2022). Fabrikasi Fe_3O_4/ZnO Nanokomposit dengan Ultrasonication Metode Gelombang dan Aplikasinya untuk Antibakteri. *Review Fisik Indonesia*, *5*(3), 177–187.

PUTRI, A. A. (2020). Sintesis dan karakterisasi bentonit terpilar logam besi dan kromium sebagai katalis untuk konversi etanol menjadi gasolin. In *Skripsi, Program Studi Kimia, FMIPA, UIN Syarif Hidayatullah Jakarta* (Vol. 21, Issue 1).

Rabiudin, R., Rusdin, R., & Maimuna, W. (2022). Telaah Kognitif: Pemetaan Kemampuan Mengingat Siswa Dalam Pembelajaran Fisika Dan Matematika. *Jambura Physics Journal*, *4*(1), 1–13. https://doi.org/10.34312/jpj.v4i1.13603

Rahimi, S. M., Panahi, A. H., Moghaddam, N. S. M., Allahyari, E., & Nasseh, N. (2022). Breaking Down of Low-Biodegradation Acid Red 206 dye using Bentonite/ Fe_3O_4/ZnO Magnetic Nanocomposite as a Novel Photo-catalyst in Presence of UV light . *Chemical Physics Letters*, *794*(139480).

Ramadhannur, A. R., Wirawan, T., & Hindryawati, N. (2021a). Fotokatalisis synthesis composite Zn-Fe_3O_4/WO_3 and their application . *Prosiding Seminar Nasional Kimia 2021*, 6–11.

Ramadhannur, A. R., Wirawan, T., & Hindryawati, N. (2021b). *Pembuatan Komposit Zn-Fe_3O_4/WO_3 dan Aplikasinya dalam Proses Fotokatalisis*. Prosiding Seminar Nasional Kimia 2021 FMIPA UNMUL.

Ramadhika, L. N., Aprilia, A., Safriani, L., Fisika, P. S., Matematika, F., Alam, P., & Padjadjaran, U. (2021). *Studi Preparasi Senyawa ZnO:TiO_2 sebagai Material Fotokatalis*. *11*(02), 83–95.

Riskiani, E., Suprihatin, I. E., & Sibarani, J. (2018). Fotokatalis Bentonit-Fe_2O_3 untuk Degradation Zat Warna Remazol Brilliant Blue. *Cakra Kimia*, *7*(1), 46–54.

Ristianingsih, Y., Istiani, A., & Irfandy, F. (2020). Kesetimbangan Adsorbsi Zat Warna Metilen Blue dengan Adsorben Karbon Aktif Tongkol Jagung Terimpregnasi Fe_2O_3. *Jurnal Teknologi Agro-Industri*, *7*(1), 47–55. https://doi.org/10.34128/jtai.v7i1.115

Suprihatin, I. E., Murdani, N. D., & Suarsa, I. W. (2021). Bentonit-Fe_3O_4 sebagai fotokatalis dalam proses fotodegradasi naphthol blue black dengan iradiasi UV. *Jurnal Kimia 15*(1), 59–66. https://doi.org/10.24843/jchem.2021.v15.i01.p09

Szostak, K., & Banach, M. (2019). Sorption and photocatalytic degradation of methylene blue on bentonite-ZnO-CuO nanocomposite. *Journal of Molecular Liquids*, *286*, 110859. https://doi.org/10.1016/j.molliq.2019.04.136

Tang, N. F. R., Tahir, D., & Heryanto, H. (2022). Sintesis Komposit ZnO/$Ca_3(PO_4)_2$ menggunakan metode Sol-gel sebagai Material Fotokatalis Limbah Cair Industri (Metilen Biru). *Jurnal Fisika Flux: Jurnal Ilmiah Fisika FMIPA Universitas Lambung Mangkurat*, *19*(1), 31. https://doi.org/10.20527/flux.v19i1.11824